Soil signature simulation of complex mixtures and particle size distributions

Tyler Carson
Charles M. Bachmann
Carl Salvaggio

SPIE.

Soil signature simulation of complex mixtures and particle size distributions

Tyler Carson,* **Charles M. Bachmann, and Carl Salvaggio**
Rochester Institute of Technology, Chester F. Carlson Center for Imaging Science, Digital Imaging and Remote Sensing Laboratory,
54 Lomb Memorial Drive, Rochester, New York 14623, United States

Abstract. Soil reflectance signatures were modeled using the digital imaging and remote sensing image generation model and Blender three-dimensional (3-D) graphic design software. Using these tools, the geometry, radiometry, and chemistry of quartz and magnetite were exploited to model the presence of particle size and porosity effects in the visible and the shortwave infrared spectrum. Using the physics engines within the Blender 3-D graphic design software, physical representations of granular soil scenes were created. Each scene characterized a specific particle distribution and density. Chemical and optical properties of pure quartz and magnetite were assigned to particles in the scene based on particle size. This work presents a model to describe an observed phase-angle dependence of beach sand density. Bidirectional reflectance signatures were simulated for targets of varying size distribution and density. This model provides validation for a phenomenological trade space between density and particle size distribution in complex, heterogeneous soil mixtures. It also confirms the suggestion that directional reflectance signatures can be defined by intimate mixtures that depend on pore spacing. The study demonstrated that by combining realistic target geometry and spectral measurements of pure quartz and magnetite, effects of soil particle size and density could be modeled without functional data fitting or rigorous analysis of material dynamics. This research does not use traditional function-based models for simulation. The combination of realistic geometry, physically viable particle structure, and first-principles ray-tracing enables the ability to represent signature changes that have been observed in experimental observations. © The Authors. Published by SPIE under a Creative Commons Attribution 3.0 Unported License. Distribution or reproduction of this work in whole or in part requires full attribution of the original publication, including its DOI. [DOI: 10.1117/1.OE.54.9.094103]

Keywords: bidirectional reflectance distribution function; phase angle; principal plane; hyperspectral.

Paper 150622 received May 13, 2015; accepted for publication Aug. 7, 2015; published online Sep. 10, 2015.

1 Introduction

In his lecture given to the Physiological Society at Chelsea College in 1970, Rushton explained the mechanisms behind human vision using the principle of univariance.[1] He stated that light sensed by rods in the retina is multivariate. Their response characteristics possess a distinct wavelength dependency and a distinct power per unit area. Yet, the output of these photoreceptors is limited to the one-dimensional parameter of brightness. The output is univariant. Wavelength only determines the proportion of incoming light that is absorbed by rods. Therefore, different combinations of wavelength and intensity can produce the same brightness.

The theory behind human vision and the principle of univariance can be applied to the spectral remote sensing of terrestrial scenes. Targets are described by many variables that contribute to a univariate measure, such as reflectance or emissivity. Target geometry is one variable. Subvariables of shape, texture, porosity, and density contribute to the geometry of a sample. Radiometry is another parameter that defines spectral characteristics. This includes features of the scene-illuminating source and the atmosphere. Chemical and optical properties should also be considered in the formula of a reflectance signature. As is the case for rods in the human eye, varied combinations of parameters could result in similar spectral reflectance signatures.

Since unidirectional measurements may not be unique, there is a chance that potential targets could be missed when spectral analysis is performed. Multiple bidirectional measurements can be employed to extract geometric, chemical, and radiometric details from a surface of interest. Making supplementary measurements at different sensing positions provides additional information that may be necessary to definitively characterize a sample. To provide a better description of the directional distribution of reflected flux, the metric of bidirectional reflectance distribution function (BRDF) can be used.[2] Defined as

$$\rho_{\text{BRDF}}(\theta_r, \phi_r, \theta_i, \phi_i, \lambda) = \frac{L(\theta_r, \phi_r, \lambda)}{E(\theta_i, \phi_i, \lambda)} [sr^{-1}]. \qquad (1)$$

BRDF is the ratio of radiance (L) reflected from a sample to the irradiance (E) from an illumination source that impinges upon that sample.

The modeling process for the BRDF of soils has taken many forms. It has been described using geometric facets,[3,4] coherent backscattering theory,[5–8] and radiative transport.[9] Differences in models exist because the relationships between geometric, radiometric, and chemical parameters are not explicitly known. This lack of knowledge is hidden through the use of data regression, which provides best-fit values for multiple undefined variables, and a final univariate solution for directional reflectance. This could mean that phenomenology has been excluded from simulation. It might also indicate that the interactions between model

*Address all correspondence to: Tyler Carson, E-mail: tdc9005@rit.edu

parameters are inappropriately related in mathematical theory. For instance, it may be difficult to determine whether certain spectral features are the byproducts of optical properties, soil geometry, or a combination of both parameters.[10] Even if optical parameters are well known, failure to integrate appropriate geometry may produce spectral signatures that do not represent measured observations.

This effort produced a simulation of the spectral reflectance and BRDF of soil. To minimize errors hidden by univariance, data fitting is not used in the simulation process. Instead, only general variables of geometry, radiometry, and chemistry are considered. The physics engine within the Blender three-dimensional (3-D) software is exploited to model geometry. The digital imaging and remote sensing image generation (DIRSIG) model is used to simulate radiometric effects. The directional hemispherical reflectance of pure materials is used to represent in-scene chemistry. Through the consideration of these three parameters, observed signature features[11–17] due to particle size, porosity, and physical mixing are closely analyzed through simulation. The ability to shed the need for functional data fitting is an important benefit of this technique.

The technique discussed in this work provides a straightforward approach to simulate intimately mixed solid materials that have not been seen in other models. By capitalizing on recent advancements in computer graphics software, complex target scenes were generated and quickly and easily manipulated. Beyond the ease of use, the target scenes are physical and are realistically posed through the use of physics engines. And because users have complete control of particle size, shape, and material makeup, this simulation method offers a convenient test bed for the study of scattering phenomenology of intimately mixed solids. Particle size distribution, shape, and density are all independently modified. It is this apparent flexibility and user control that makes this simulation scheme unique.

1.1 Phenomenology

Soil particles are composed mostly of rock-forming minerals. These substances are subjected to weathering and the impact of human activities. Under different conditions of exposure, soil-packing density is known to change. Defined by particle size and shape, the grain spacing, or porosity, will impose limitations on soil density. Documentation reveals that changes in geometry and porosity have an impact upon reflectance.[5–16] Even so, the exact relationship between porosity and reflectance is still ambiguous. Laboratory studies have shown that reflectance does increase with density.[12–16] In other observations, porous soils were more reflective than those that were more dense.[11] The Hapke reflectance model indicates that there is a direct relationship linking the increases in density and the increased levels of measured radiance.[9] Others have expressed that porosity may affect measurements only on a secondary level, and that chemistry and particle geometry may be more impactful.[17]

It may be inappropriate to define an independent proportionality relationship between soil density and reflectance since soils are generally not homogeneous. Hapke has incorporated mixed materials into BRDF modeling by treating a surface as a weighted combination of single scattering albedos.[18] This model accounts for density and particle diameter, but assumes isotropic scattering within the

mixture. The uncertainty inherent in the assumption of isotropic scatter may be important. It was shown that the current form of the Hapke model is not invertible, indicating that the relationships between some of the geometric and chemical reflectance parameters may not be well defined.[16] The intimate mixing process that is observed in nature is not isotropic. Commonly encountered soils often consist of mixtures of translucent and opaque materials. Layered soils have varying density, and there regularly exists low-density particle dusting on many surfaces.[17,19] Attempts to decompose univariant reflectance into its subparameters have relied on the assumption of relatively narrow size distributions. Uniform material samples can have widely varying size distribution. Particles with diameters on the order of tens of microns have been shown to cling to larger particles when in the presence of electrostatic forces.[17,19] Pore spacing is certainly dependent upon particle size distribution. Decreases in particle size have been shown to increase the density within a single material.[12,16] However, the trade-space among density, physical particle mixing, and nonisotropic particle size distributions has not been thoroughly explored in the modeling realm.

Directional reflectance has been used in studies of the geometric scattering parameters of mixed soil. Bachmann et al. measured beach sand samples of different densities to observe reflectance trends related to changing phase angle.[11] Phase angle is the angle subtended by illumination source, sample, and a sensor. It was observed that lower density sands had larger reflectance than higher density sands. The trend became more pronounced as the phase angle increased. Reflectance contrast was observed at visible wavelengths, but it was even more pronounced as wavelength increased. The soil used in this experiment was composed predominantly of quartz and opaque magnetite. Quartz grains had diameters on the order of hundreds of microns, while the magnetite particles were generally smaller than 75 μm. The conjecture of the work was that the small, absorbing, magnetite particles more completely filled the pores of the soil under dense geometric configurations, reducing multiple scattering contributions to the overall observed reflectance.

1.2 Modeling Phenomenology

The geometric assumption that was made above to describe reflectance phenomenology is difficult to prove in the laboratory. To understand it completely, one would need to compare similar size distributions of quartz soil and composite soil containing quartz and magnetite grains. Ideally, the density of each sample should be the same. With fixed parameters of density and size distribution, any change in reflectance could be attributed to the presence of magnetite. Then, the impact of changing density could be teased out by comparing the BRDF of high-density and low-density quartz and composite soil. If the conjectures of Bachmann et al. are true, more variance should be present in the high-density BRDF data than in the low-density data. The high-density scene of composite soil should have a lower observed reflectance than that of low-density quartz or composite soil.

The function fit models of Refs. 4 and 9 do not contain the accurate descriptions of intimate mixing or geometric versatility required to simulate the observations of the Bachmann et al. experiment. The work of Cierniewski et al.

employed 3-D graphics models to simulate sample soil scenes.[20,21] However, the surface irregularities used in these models were based on periodic mathematical functions and could not be used to explore the geometric specifics of particle size distribution and porosity. This work describes a simulation that pairs physically realistic granular targets (created using Blender 3-D graphic design software) and the DIRSIG model to create virtual signatures of soils with changing porosity, size distribution, and material properties.

1.3 Modeling with Digital Imaging Remote Sensing Image Generation and Blender Three-Dimension

It is important to state what this model is not. The method used in this work is not an attempt to mathematically integrate all of the variables and processes that result in the univariate measure of reflectance. It does not explicitly calculate reflectance from optical properties. It is not a parameter-based model containing arbitrary functions that are fit to data curves. This model does not define surface geometry as a probabilistic distribution of facets[4] or isotropic bulk densities.[9,18] It does not assume that a scene of thousands of irregular particles will scatter as a linear or weighted combination of individual phase functions solved independently of one another.[9,18]

This is a model, which is focused on scene geometry and simulates the reflectance of the complex mixtures of solids. This is an avenue to explore the phenomenology of particle size distribution, density, and intimate mixing. Most importantly, the model easily bundles together the chemical, radiometric, and geometric components of material signatures.

Chemical parameters to be considered in a complete soil scattering model would include indices of refraction, absorption, anomalous dispersion, anisotropy, and lattice vibrations. Instead of attempting to calculate all of these parameters in parallel, measured reflectance spectra of pure materials are used in this simulation procedure. For instance, quartz particles in this model that possess a 500 μm radius are attributed with the measured spectra of 500 μm quartz. By using pure spectra, many of the problems associated with modeling the integration of chemistry, geometry, and radiometry are eased.

The radiometric aspects of this simulation are solved using the DIRSIG model. DIRSIG is a first-principles ray-tracing model that outputs detected at-sensor radiance. Light sources, scene geometries, and sensor configurations are all defined by the user (Fig. 1). This model has been predominantly used for the analysis and modeling of sensors. DIRSIG allows for direct system comparisons. A single scene can be observed under varying atmospheric conditions, with multimodal sensing techniques. Though it is easy to conceptualize passive remote sensing as light rays traveling from source to target to sensor, DIRSIG models radiation in inverse fashion. Rays are initially cast from individual pixels of a user-defined focal plane array. These rays determine the area observed at each pixel, and where incident radiation originates.

The geometry of soil is created using the Blender 3-D open source graphic design software. This design suite gives users the ability to etch, bend, and connect different shapes or planes to create objects with precision. Using built-in physics engines, one can create a scene of objects that interact based on the physical properties (mass and
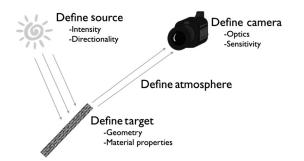

Fig. 1 The versatility of digital imaging and remote sensing image generation (DIRSIG) lies in user control. Within a single simulation, each link of the image chain can be modeled with precision. The input of the chain is a uniquely defined scene and irradiance level. The output is a radiance image produced by a virtual sensor. Links of the chain include the light source, radiation propagation, target geometry, atmosphere, and the sensor. Parameters of each link are defined prior to simulation. Since the model is compartmentalized, scenarios can be changed with precision and with ease.

shape) defined by the user. Simulation of rigid body collisions, fluid motion, and force field interactions is possible using the Blender 3-D tool. Each mesh object is subjected to friction and damping, and interacts with other objects through collisions based on mass. Individual mesh facets influence collisions between in-scene objects. This implies that a convex hull does not define the physical bounds of a soil particle created in Blender 3-D. For instance, a multifaceted particle is bounded by its facets rather than a sphere or a six-sided cube with similar volume.

2 Methods

2.1 Geometry

This model of beach sand begins with a geometric description at the microscopic level. As alluded to in the introduction, mesh objects of different geometries are rotated, translated, and extruded to produce objects that match the 3-D geometry of soil grains. Scanning electron microscope images provided a visual template for particle design.

In this work, the parameter of particle size distribution is defined using sand that was collected from the Virginia Coast Reserve Long-Term Ecological Research project (VCR-LTER).[22,23] The distributions used in this experiment are shown as histograms in Fig. 2. Each distribution was collected at a different transect of the same site on North Smith Island, Virginia. Soil samples were sieved to separate particles and weighed to determine the percentage of each particle size within the sample. Three different distributions were used for this model. As seen in Fig. 2, distribution (a) was nearly uniform. Particles within this distribution ranged in diameter from 10 to 600 μm. Distribution (b) was a bimodal distribution. Particles from this sample ranged in diameter from 100 to 600 μm. Greater than 70% of the particles in the scene were either 150 μm or 600 μm in diameter. Samples from the Bachmann et al. measurements most closely mimicked distribution (b). Distribution (c) was practically unimodal with greater than 70% or the particles having a diameter of approximately 150 μm.

Realistic pose and mixture of scene constituents were created with the Blender 3-D physics engine. To model a natural soil scene, particles were not individually placed by hand.
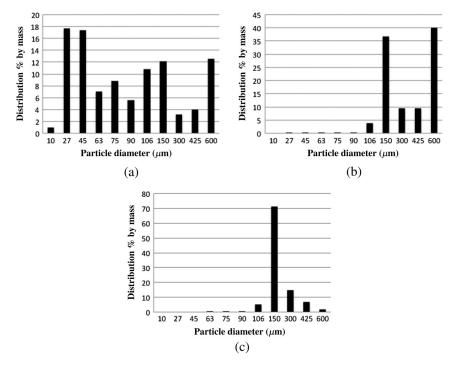
Fig. 2 Scenes used within the DIRSIG simulations were fashioned using three particle size distributions. Distribution (a) was more uniform with respect to particle diameter. Distribution (b) was bimodal with the majority of particles possessing diameters between 150 and 600 μm. More than 70% of particles in unimodal distribution (c) had a diameter of 150 μm.

User placement of thousands of objects would be incredibly tedious and would likely produce an unphysical result. Each particle was treated as a rigid body and was dropped onto a surface where particle interactions occurred. Grains eventually settled into a physical 3-D soil scene. This process was performed for each particle size distribution and is illustrated in Fig. 3.

Within the Blender 3-D graphic design software, this soil scene simulation takes the form of a motion picture. At each frame, particle position was calculated using the mass, shape, and external forces of gravity and interparticle collisions. A single frame was used to describe the target, and was provided as input to the DIRSIG radiometry solver. This geometry included the position in x, y, z coordinates of all object vertices. It is an actual record of particle shape and position that forms an accurate account of particle distribution and spacing.

The density of the scene was altered by the addition of more particles. The change in density was calculated using a volumetric bounding box within the Blender 3-D software. Af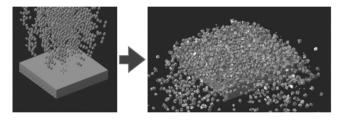ter the rigid body physics engine was applied, the number of particles within a bounded volume was calculated. Figure 4 shows the geometric representation of two particle scenes that have the same size distribution [distribution (b)], but differ in grain density by 29%.

2.2 Chemistry

Before each geometric scene was inserted into a DIRSIG radiometric simulation, spectra were assigned to the facets of each particle. Spectral reflectance and emissivity response curves represent how each facet will respond to interaction with a photon. Absolute reflectance of pure quartz was assigned to each particle in both the high- and low-density configurations for the distributions shown in Figs. 2(a) to 2(c). A total of six quartz scenes were considered. Both high- and low-density scenes were developed for each of the three particle size distributions.

To investigate the impact that soil density has upon the spectral signature of a mixed soil sample, reflectance properties of both magnetite and quartz were included in a single scene. A high-density scene and a low-density scene of mixed soil were created. The trends observed by Bachmann et al.[11] were thought to be a byproduct of smaller magnetite grains physically mixed with larger quartz grains. Therefore, the distribution shown in Fig. 2(b) was used for each of the two mixed scenes. As seen in Fig. 5, the smallest particles (106 and 150 μm) were given the spectral signature of magnetite. All particles larger than 150 μm were attributed with the absolute reflectance of pure quartz.

Spectral reflectance data were obtained from a spectral material library hosted by the United States Geological Survey (USGS). This database contains reflectance information for natural minerals and flora, as well as manmade surfaces and complex mixtures.[24]
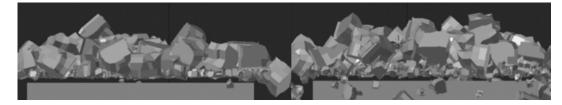

Fig. 3 The process of scene building is based upon physics engines in the Blender 3-D graphic design software. Particles fall onto a surface where they settle naturally in space. A sample motion picture of particles can be viewed online.[29]

Fig. 4 The scene on the right was 29% more dense than the scene on the left. Pores in the high-density scene are more completely filled than those corresponding to the low-density target.

2.3 Radiometry

In Eq. (1), L describes the radiance reaching the sensor produced by a DIRSIG simulation. This radiance comprised many components that are included within the governing equation

$$
\begin{aligned}
L(\lambda, \theta_v, \phi_v, \theta_l, \phi_l) \\
= \frac{E_l(\lambda)}{\pi} \cos(\theta_l) \tau_1(\lambda, \theta_l) \rho(\lambda, \theta_v, \phi_v, \theta_l, \phi_l) \tau_2(\lambda, \theta_v) \\
+ L_u(\lambda, \theta_v),
\end{aligned} \tag{2}
$$

with the angular orientation of the solar light source represented by zenith angle θ_l, and by azimuthal angle ϕ_l. The sensor viewing position is described using (θ_v, ϕ_v). E_l defines the irradiance that is emitted from a single light source. The spectral BRDF $\rho(\lambda, \theta_v, \phi_v, \theta_l, \phi_l)$ depends on the directionality of both the sensor and the light source. Transmission of radiation is denoted by τ. The radiation paths to and from the target are considered separately using two transmission terms. Additional upwelling path radiance is represented as L_u.

The user control of light sources and sensors allows for the BRDF, as shown in Eq. (1), to be found painlessly. Radiance, L, from the governing equation above, is the output of each DIRSIG simulation. Virtual DIRSIG sensors do not exhibit perfect sensitivity at all wavelengths. Every simulation photon that hits a detector does not necessarily result in a signal electron. Therefore, solving for BRDF requires compensation for device sensitivity. Detectors typically have spectral response functions that describe how
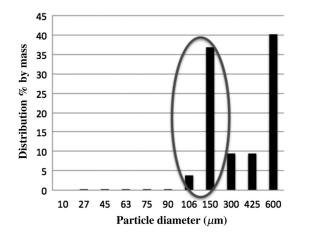
efficiently photons are converted into signal over a range of wavelengths. The virtual sensor used in this experiment was characterized by Gaussian-shaped response functions centered at 450, 550, 650, 868, 1000, and 1915 nm. Bachmann et al. [11] also analyzed spectral reflectance at these wavelengths. Half nanometer spectral resolution was used. The virtual sensor was positioned 1.78 m from the virtual soil surface. A reduced instantaneous field of view (IFOV) of 0.092 m was evaluated in an attempt to maintain a constant view of the scene as the sensor zenith angle was increased. This sensor configuration matches that of the University of Lethbridge goniometer system version 2.5 (ULGS-2.5).[25] Prior to simulation, the total scene irradiance, E, is specified by the user. The solar illumination source was initially positioned with a zenith angle of 30 deg from nadir. Scenes with a solar zenith angle of 20 deg were also subjected to simulation. DIRSIG will not allow for remotely sensed signal to exceed that of the illumination source.

Using the scenes and modeling techniques described above, the BRDF of pure quartz and mixed soils can be modeled. BRDF was calculated for samples of quartz, having different particle size distributions and density. Additional BRDF models were simulated for samples of mixed quartz and magnetite. Within each scene, rays are traced from the illumination source, to the soil sample, and then on to the sensor. Light often interacts with multiple grain boundaries as it travels. At times, these grains are different materials that possess unique chemical and optical properties. The result is a reflectance signature that represents the intimate mixing of chemical properties within the sensor IFOV.

3 Results

BRDF values were simulated for quartz scenes at intervals of 20 deg between zenith angles of -60 deg and 60 deg in the principal and perpendicular planes. These two measurement planes are defined by the positions of the illumination source and the virtual sensor. Measurements are said to be in the principal plane if the source and sensor share the same azimuth angle or if the source and sensor have azimuth angles that are separated by 180 deg. In the perpendicular plane, the sensor azimuth is positioned 90 deg from the source azimuth. Both measurement scenarios are illustrated in Fig. 6.

For soil targets, the backscatter direction of the principal plane is often defined by a reflectance peak that is maximized near the solar zenith angle.[24–26] This preferential scattering is due to an absence of particle shadowing and occlusion within the line of sight between the sensor and the sample. Unique reflectance features also arise from the intimate mixing of grains, scattering albedo, grain transmittance, and sample density. The reflectance signature of the perpendicular plane
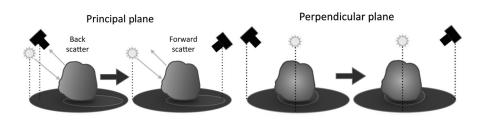

Fig. 5 Distribution (b) from Fig. 2 was used to describe a mixture of quartz and magnetite. Particles with 106 and 150 μm were attributed with the spectral properties of magnetite. Larger particles were represented as quartz in the DIRSIG simulations.

Fig. 6 Principal plane (a) measurements are made when a light source and a sensor have the same azimuth angle or when the source and sensor have azimuth angles that are 180 deg apart. In the perpendicular plane (b), the least amount of shadowing and occlusion is observed when the sensor is directly above the target. Because the light source is located in a plane that is perpendicular to the sensor, the reflectance decreases uniformly as the sensor zenith angle is increased from the nadir position. Darkness dominates the shadowed regions of a target, resulting in fewer reflected rays traveling between the target and the sensor. Reduced spectral contrast is a byproduct of these shadows. Unique reflectance features also arise from the intimate mixing of grains, scattering albedo, grain transmittance, and sample density.

has been observed as a bell curve with the maximum occurring where the sample is sensed at nadir.[25,27] Signal drops off fairly uniformly as the sensing zenith angle increases, because shadowing changes very little when the sensor is moved along the azimuthal axis perpendicular to the sun. This can be observed in Fig. 6.

Results of the quartz simulation agree with the expected scattering characteristics described above. Figure 7 shows the directional signatures of the quartz scenes in the principal and the perpendicular planes. For each of the three distributions, the low-density simulation results are plotted with the high-density results. BRDF percentage is plotted against sensor zenith angle. The position of the illumination source is indicated in plots of the principal plane. The data provide some interesting insights on particle size distribution. As previously stated, the relationship between soil density and reflectance has been modeled and observed with some variance in results. Several observations indicated that a dense geometry of soil is more reflective than a sample with lower density.[12–16] Models have confirmed this result.[9] However, observations by Bachmann et al. indicate that the relationship between density and reflectance may be more complicated.[11]

The model results displayed in Fig. 7 support both claims. The signature gathered from the uniform distribution [Fig. 2(a)] indicates that at backscattering view angles, the dense sample is more reflective than quartz that is less dense. As the sensor moves to positions associated with forward scattering, less dense soil is more reflective. It is also noted that reflectance falloff in the perpendicular plane is not

truly uniform. This indicates that particle geometry and size distribution have an observable effect on soil signatures. For a sample that contains particles of many sizes, such as the uniformly distributed soil, it is likely that much of the available pore space will be filled as soil settles. At higher densities, pores may fill completely. This results in a varied distribution of large and small particles at the topsoil layer. In the backscatter direction, porous light traps become rare and smaller particles can be sensed. In the forward scattering direction, shadowing is prevalent. Any light that does bounce from small grains into the forward scattering direction will likely be blocked by large particles before it can reach the sensor. If a sample of the same distribution was less dense, larger grains would dominate the geometry of the topsoil and shadowing in the forward direction would be less severe. These trends are observed in the results corresponding to the uniform distribution of quartz, and they are displayed in Fig. 7.

A different trend is evident when the geometry of the soil surface is represented by the bimodal and unimodal distributions. Lower density samples of both distributions were modeled to have stronger reflectance signatures than more dense samples of the same distribution (Fig. 8). This implies that for the samples in this experiment, pore spacing was measureable. In the scenes depicting dense soil representations of these narrow size distributions, grains on the very top surface of the sample tended to settle relatively far from one another. This geometric separation of large particles resulted in an observable variance in surface height. When bimodal and unimodal distributions were used in less dense Blender 3-D
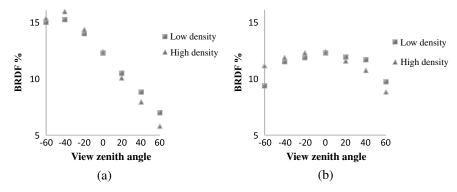

(a)

(b)

Fig. 7 Bidirectional reflectance distribution function (BRDF) of quartz at 650 nm is plotted in the principle plane (a) and perpendicular plane (b) for a uniform particle size distribution. The effect of density on BRDF varies based on sensor location.
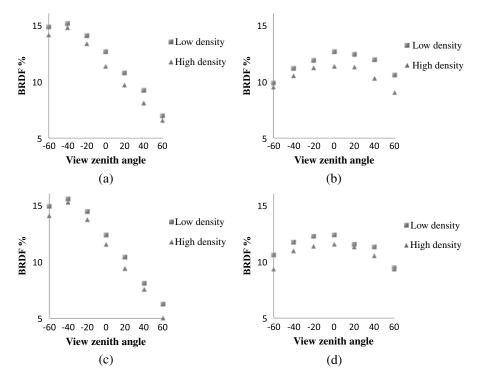
Fig. 8 BRDF at 650 nm is plotted in the principal plane (a,c) and perpendicular plane (b,d) for a bimodal particle size distribution (a,b) and a unimodal particle size distribution (c,d). In both scenarios, low-density soil appears more reflective than high-density soil.

scenes, grains at the top surface were more tightly grouped. The change of top surface height in these scenes was less severe. This difference in topsoil surface height has been previously used in physical optics-based BRDF models and is referred to as effective surface roughness.[28] This implies that even if the same particle size distribution is manifested in two separate samples, these samples can have different surface texture. Such a change ultimately alters the level of measured signal. It explains how a less dense sample, with a very specific particle size distribution, will be observed to be more reflective than soil with higher density.

An additional test was performed to explore the reliability of the aforementioned results. To ensure that the trends shown in Figs. 7 and 8 were not simply the product of unique geometry, additional simulations with different geometric deposition were carried out and the variability of the

produced reflectance was calculated. Three additional scenes were created using the Blender 3-D physics engines. The bimodal particle size distribution was used in each scene. The same number of particles was used in each scene. The only difference between the simulations was the initial positioning of the rigid body particles prior to implementation of the physics engine. Standard deviations were calculated for each BRDF value. This deviation is plotted with the original BRDF results in Fig. 9. There was overlap between the standard deviations of the low- and high-density quartz signatures. Only three of the 14 low-density data points were within a standard deviation of the high-density trend line. The model seems to consistently predict that a low-density sample of quartz that is defined by the aforementioned bimodal distribution will reflect more light than a higher density soil that shares the same distribution.
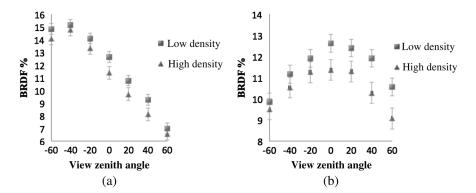

Fig. 9 Mean and standard deviation from three separate scenes of similar particle size distribution and density were plotted in the (a) principal and (b) perpendicular planes. The lack of overlap in the trend lines suggests that the model will consistently predict that soil samples with size distribution b will be more reflective in low-density scenarios.

The bimodal particle size distribution was used to evaluate the effects of density for soil samples that contained a mixture of quartz and magnetite particles. Within the Blender 3-D sample, small particles (106 and 150 μm) were given the spectral signature of magnetite. All particles larger than 150 μm were represented as pure quartz. This distribution was used because it closely resembled the distribution observed by Bachmann et al.[11] In that paper, soil that was denser was observed to reflect less than sand with higher levels of porosity. It was assumed that this result was a consequence of small black magnetite particles that more completely fill pore spaces when soil is dense. To test this,

a DIRSIG simulation was created using the scene described above. The illumination source was positioned 20 deg from nadir in the zenith axis. BRDF values were calculated in the visible and shortwave infrared (SWIR). The reflectance characteristics of the mixed soil are compared with pure quartz in Fig. 10.

This DIRSIG-based model shows that the results observed by Bachmann et al. may have been partially caused by the particle size distribution of the sample soil. The plots in Fig. 10 also confirm the notion that the effects of magnetite are more pronounced in high-density samples. Figures 10(a) to 10(c) correspond to a high-density soil sample and reveal a
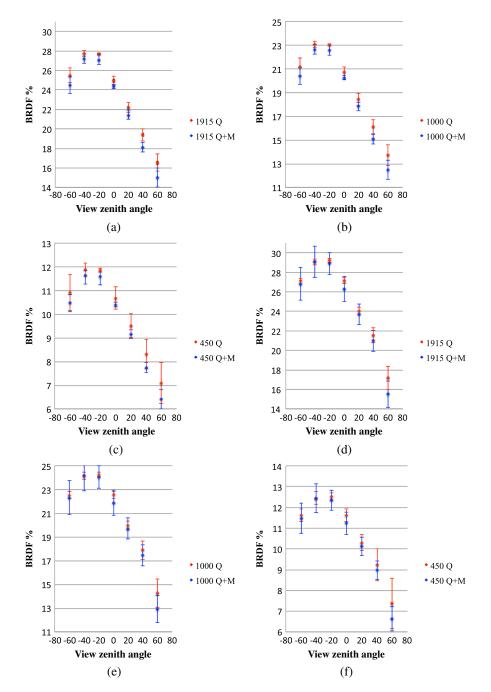

Fig. 10 BRDF results from different mixture and density scenarios were plotted in the principal plane at 1915, 1000, and 450 nm. In the high-density plots (a-c), the impact of intimate mixing between magnetite and quartz was defined by a noticeable drop in reflectance at all viewing angles. There was very little variance between the BRDF of mixed soil and pure quartz in the low-density scenario (d-f).
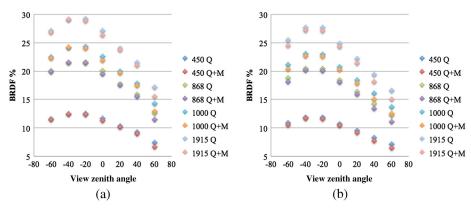
Fig. 11 Principal plane BRDF of bimodal quartz and a bimodal quartz/magnetite mixture is plotted at 450, 868, 1000, and 1915 nm for low-density (a) and higher density (b) scenarios. As observed by Ref. 11, the difference in BRDF between the pure and mixed targets increases when density is high.

noticeable decrease in the reflectance of soil containing small magnetite grains. A much smaller reflectance gradient exists in Figs. 10(d) to 10(f), which describe a low-density sample. Bachmann et al. also observed there to be greater variance in measurements collected in the SWIR. The spectral reflectance of quartz contrasts more with the reflectance of magnetite in this regime.[11] This trend is observed in the simulation results displayed in Fig. 10. All plots in this figure include standard deviation error bars, which were calculated using the reflectance simulation of five separate geometric representations of the respective high- and low-density scenes. Standard deviation is larger in the low-density scene. Not only is the reflectance gradient in the 450, 1000, and 1915 nm bands less distinct for the less-dense scene, there is less certainty in the results. This is a product of transient porosity features in the five different simulations of the low-density scene. There was less change in porosity between each representation of the high-density scene. BRDF change with respect to wavelength can be seen in Fig. 11, where the 450, 868, 1000, and 1915 nm bands are plotted together for low-density [Fig. 11(a)] and high-density [Fig. 11(b)] scenarios.

For a bimodal distribution, spectral contrast due to density has been observed to increase as phase angle increases.[11] The DIRSIG model presented in this work also predicts this tendency. Figure 12 shows that the increase in contrast of a quartz and magnetite mixture occurs at visible and SWIR wavelengths. As expected, contrast is greater in the SWIR and increases with larger phase angles. This simulation did not consider coherent scatter beyond that which was captured in the reflectance measurements of the USGS. Therefore, the trend of increasing contrast that was observed in Ref. 11 can be at least partially attributed to the intricacies of soil geometry that are associated with pore spacing, particle size, and surface texture.

4 Conclusion

Using Blender 3-D and DIRSIG, geometric aspects of soil samples were studied with precision. The physical relationships between density, particle size, and intimate material mixing were shown to validate notions of increased soil reflectance with decreased density (increased porosity) as previously observed in laboratory studies.[11] It was shown that the presence of small magnetite grains will have a larger impact upon reflectance if a sample is more dense, further decreasing reflectance as conjectured in the earlier study.[11]

Additionally, the degree of contrast in reflectance signature that increases with phase angle was linked to sample geometry. Models affirmed that the univariant signature of reflectance is built upon an interdependent trade space of several geometric variables. The influence of realistic particle geometry needs to be explored in greater depth if functional models are to be accurately developed for soils and mixed solids. It is the ability to focus on geometric modeling that separates this technique from other models. Because the use of Blender 3-D and DIRSIG provides complete user control of sample geometry and the assignment of spectral properties, it serves as a convenient test-bed for target construction and target signature sensing. This technique can be easily modified for implementation with other material mixtures provided that pure spectral reflectance or emissivity data is available. Ultimately, this study demonstrated that by combining
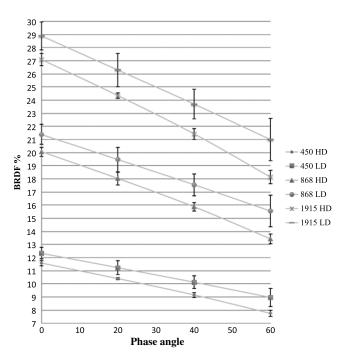

Fig. 12 Variance between the reflectance of high-density soil and low-density soil for a bimodal distribution of magnetite and quartz was shown to increase as phase angle increased. The effect was more dramatic in the shortwave infrared (SWIR). These effects have been observed in previous lab analysis.[11]

realistic target geometry and spectral measurements of pure quartz and magnetite, effects of soil particle size, density, and texture could be modeled without functional data fitting or rigorous analysis of material dynamics.

Acknowledgments

References

1. W. A. H. Rushton, "Review lecture. Pigments and signals in colour vision," *J. Physiol.* **220**(3), 1–31 (1972).
2. F. E. Nicodemus, J. C. Richmond, and J. J. Hsia, *Geometrical Considerations and Nomenclature for Reflectance*, U.S. Department of Commerce, National Bureau of Standards, Washington, DC (1977).
3. K. E. Torrance and E. M. Sparrow, "Theory for off-specular reflection from roughened surfaces," *J. Opt. Soc. Am.* **57**(9), 1105–1112 (1967).
4. J. R. Maxwell et al., *Bidirectional Reflectance Model Validation and Utilization*, Environmental Research Institute of Michigan, Ann Arbor, Michigan, 196400-1-T (1973).
5. M. I. Mischenko et al., "Bidirectional reflectance of flat, optically thick particulate layers: an efficient radiative transfer solution and applications to snow and soil surfaces," *J. Quant. Spectrosc. Radiat. Transfer* **63**, 409–432 (1999).
6. M. I. Mischenko, L. D. Travis, and A. A. Lacis, *Multiple Scattering of Light by Particles: Radiative Transfer and Coherent Backscattering*, Cambridge University Press, New York (2006).
7. J. M. Dlugach et al., "Numerically exact computer simulations of light scattering by densely packed, random particulate media," *J. Quant. Spectrosc. Radiat. Transfer* **112**, 2068–2078 (2011).
8. V. P. Tishkovets, E. V. Petrova, and M. L. Mischenko, "Scattering of electromagnetic waves by ensembles of particles and discrete random media," *J. Quant. Spectrosc. Radiat. Transfer* **112**, 2095–2127 (2011).
9. B. W. Hapke, Ed., *Theory of Reflectance and Emittance Spectroscopy*, 2nd ed., Cambridge University Press, New York (2012).
10. J. E. Moersch and P. R. Christensen., "Thermal emission from particulate surfaces: a comparison of scattering models with measured spectra," *J. Geophys. Res.* **100**(E4), 7465–7477 (1995).
11. C. M. Bachmann et al., "Phase angle dependence of sand density observable in hyperspectral reflectance," *Remote Sensing Environ.* **150**, 53–65 (2014).
12. F. Capaccioni et al., "Phase curves of meteorites and terrestrial rocks: laboratory measurements and applications to asteroids," *Icarus* **83**, 325–348 (1990).
13. G. Georgiev et al., "BRDF analysis of savanna vegetation and salt-pan samples," *IEEE Trans. Geosci. Remote Sens.* **47**, 2546–2556 (2009).
14. S. Kaasalainen, "Laboratory photometry of planetary regolith analogs. I. Effects of grain and packing properties on opposition effect," *Astron. Astrophys.* **409**, 765–769 (2003).
15. J. A. M. Dematt et al., "Soil density evaluated by spectral reflectance as an evidence of compaction effects," *Int. J. Remote Sens.* **31**(2), 403–422 (2010).
16. M. K. Shepard and P. Helfenstein, "A laboratory study of the bidirectional reflectance from particulate samples," *Icarus* **215**(2), 526–533 (2011).
17. J. Salisbury and A. Wald, "The role of volume scattering in reducing spectral contrast of reststrahlen bands in spectra of powdered minerals," *Icarus* **96**, 121–128 (1992).
18. B. W. Hapke, "Bidirectional reflectance spectroscopy 7: the single particle phase function hockey stick relation," *Icarus* **221**, 1079–1083 (2012).
19. J. R. Johnson et al., "Infrared measurements of pristine and disturbed soils 1. Spectral contrast differences between field and laboratory data," *Remote Sens. Environ.* **64**, 34–46 (1998).
20. J. Cierniewski and M. Gulinski, "Furrow microrelief influence on the directional hyperspectral reflectance of soil at various illumination and observation conditions," *IEEE Trans. Geosci. Remote Sens.* **48**, 4143–4148 (2010).
21. J. Cierniewski, T. Gdala, and A. Karnieli, "A hemispherical-directional reflectance model as a tool for understanding image distinctions between cultivated and uncultivated bare surfaces," *Remote Sens. Environ.* **90**, 505–523 (2004).
22. C. M. Bachmann et al., "Virginia Coast Reserve 2007 remote sensing experiment," NRL/MR/7230-12-9402, p. 169 (2012), http://www.dtic.mil/docs/citations/ADA559955.
23. C. M. Bachmann et al., "Retrieval of substrate bearing strength from hyperspectral imagery during the Virginia coast reserve (VCR '07) multi-sensor campaign," *Mar. Geod.* **33**(2–3), 101–116 (2010).
24. R. N. Clark et al., USGS digital spectral library splib06a: U.S. Geological Survey, Digital Data Series 231, http://speclab.cr.usgs.gov/spectral.lib06 (2007).
25. Z. Wang et al., "Assessment of soil surface BRDF using an imaging spectrometer," *Proc. SPIE* **7830**, 783010 (2010).
26. J. Cierniewski and M. Verbrugghe, "Influence of soil surface roughness on soil bidirectional reflectance," *Int. J. Remote Sens.* **18**(6), 1277–1288 (1997).
27. C. Bacour and F. M. Bréon, "Variability of biome reflectance directional signatures as seen by POLDER," *Remote Sens. Environ.* **98**, 80–95 (2005).
28. X. D. He et al., "A comprehensive physical model for light reflection," *Comp. Graphics* **25**(4), 175–186 (1991).
29. http://www.cis.rit.edu/~cnspci/media/publications/video/spie9461-62_figure1.php.

Tyler Carson is a PhD candidate at the Rochester Institute of Technology. He earned his BS in physics from the University of Northern Colorado and gained an Air Force commission through ROTC in 2009. He holds an MS from the University of New Mexico Optical Science & Engineering program. He has worked previously at the Air Force Research Laboratory, where he developed novel solid-state lasers and optically pumped semiconductor laser devices.

Charles M. Bachmann received the AB in physics from Princeton University in 1984 and the ScM and PhD degrees in physics from Brown University in 1986 and 1990. From 1990 to 2013, he was a researcher at the US Naval Research Laboratory. Since 2013, he has been Frederick and Anna B. Wiedman Chair and Associate Professor in the Digital Imaging and Remote Sensing Laboratory of the Chester F. Carlson Center for Imaging Science, Rochester Institute of Technology.

Carl Salvaggio holds BS and MS degrees in imaging science from the Rochester Institute of Technology (RIT) in 1987. He received his PhD in environmental resource engineering in 1994 from the State University of New York, College of Environmental Science and Forestry, at Syracuse University. From 1994 to 2002 he worked on model validation and database development for the defense intelligence community. Since 2002 he has been a professor of imaging science at RIT.